Design of Wideband Quad-Ridged Waveguide Orthomode Transducer at L-Band

Jin Fan[1, 2, 3, *], Yihua Yan[3, 4], Chengjin Jin[1, 2], Dezhi Zhan[1, 2], and Jirun Luo[3, 5]

Abstract—In this paper, an L-band wideband quad-ridged waveguide orthomode transducer (OMT) for the Five hundred meter Aperture Spherical radio Telescope (FAST) is presented with a simple design principle. By designing two critical parts of the OMT separately and introducing matching rings into two orthogonal probes, an improved wideband performance has been realized successfully. The OMT is designed to operate across the 0.95 GHz–1.9 GHz band, and the simulation shows a return loss better than −20 dB for both polarizations, cross-polarized isolation levels over 45 dB and insertion loss lower than 0.15 dB over the entire bandwidth. The measured results are in good agreement with the simulations.

1. INTRODUCTION

The orthomode transducer (OMT), which is an important component in both radio astronomy and telecommunication applications, is used to separate orthogonal modes in a waveguide into two waveguides or transmission lines within the same frequency band. With the development of broadband corrugated feed horns, the design of wideband orthomode transducers is demanded. Several different broadband OMT types have been presented in previous works, including the coupled waveguide [1, 2], finline [3, 4], planar [5], and quad-ridged waveguide types [4, 6–11].

The coupled waveguide OMT in [1], with a small return loss less than −20 dB and a high isolation over 50 dB, could be scaled to millimeter wave application due to its simple structure and low loss properties, but is difficult to achieve a bandwidth wider than 1.5 : 1 [2]. The basic concept of finline OMT was discussed by Robertson [3] in 1956, in which the impedance matching was improved with a return loss less than −15 dB over the bandwidth of 1.7 : 1; however the asymmetric structure made the maximum relative cross-polar level exceed −20 dB, which limits the application of the finline OMT [4]. In [5], a compact planar OMT was presented with a cross-polarization at a level below −58 dB as well as a return loss less than −20 dB over a 1.5 : 1 bandwidth. However, a 180° hybrid and dielectric substrate are needed in this design, which inevitably introduce additional insertion loss.

The quad-ridged waveguide OMT was studied in [4], and a wide bandwidth close to 2.2 : 1 can be achieved with a return loss less than −15 dB, but cross-polarization isolation was limited to 25 dB or less [6]. Some improved designs for the quad-ridged waveguide OMT were proposed in order to improve the return loss and isolation performances [7–10]. The techniques mainly include: introducing absorber and shorting blocks to improve in-band properties [7, 8] and offsetting the ridge tapers to increase single-mode bandwidth [9, 10]. In [8], by introducing absorber and shorting blocks in the structure, the EVLA L-Band OMT offers a full octave bandwidth performance with a return loss not larger than −18.8 dB

and cross-polarization isolation better than 35.7 dB. In [9], the OMT performed well from 2.4 GHz to 4 GHz (1.7 : 1) with a return loss below −20 dB and cross coupling below −40 dB when the ridge tapers were offset along the propagation direction. In [10], an improved offset quad-ridged OMT with 3.4 : 1 bandwidth was proposed with −15 dB return loss, 50 dB isolation and 0.2 dB insertion loss, and it should be the widest-bandwidth OMT to the authors' knowledge. However, there are many parameters to be optimized for this type of OMT, including the splines profile of the ridges both in height and width as well as the profile of the outer wall, which may increase the complexity of the OMT design and manufacture.

In this paper, we aim at developing a wideband orthomode transducer at L-band for the FAST telescope, which has been built in a KARST depression in Guizhou Province in the southwest part of China. FAST focuses on surveying the neutral hydrogen line in distant galaxies out to very large redshifts, looking for the first shining star, and detecting thousands of new pulsars [12]. The main technical specifications for FAST at L-band are sensitivity with $A/T \sim 1500 \, \mathrm{m^2/K}$ and $T_{sys} \sim 25 \, \mathrm{K}$. The frequency range for the OMT is from 1.1 GHz to 1.9 GHz (connecting to a corrugated horn), with a return loss less than −20 dB and cross-polarized isolation above 40 dB. Moreover, the OMT may need to present a low insertion loss so that low noise temperature can be achieved. Besides these, ease in manufacturability processing and assembly are also the main criteria in this OMT design.

This FAST OMT design is subject to stringent specifications. To meet these specifications, the design of an improved wideband quad-ridged waveguide OMT is proposed in the following parts. At first, the structure of the proposed OMT is described, and then design principle and mechanism of the OMT are elaborated. Finally the wideband OMT prototype is manufactured and measured to provide experimental verification for the simulated results.

2. THE STRUCTURE OF THE OMT

The structure of the OMT is shown in Fig. 1, and this OMT can be divided into two sections for analysis. The first OMT section is the coaxial to the constant cross-sectional quad-ridged waveguide transition (left to AA′ as seen in Fig. 1(a)). The next section is the tapered quad-ridged to the circular waveguide transition (right to AA′ as seen in Fig. 1(a)).

The OMT adopts a circular quad-ridged waveguide and is fed by two coaxial lines through the ridges, with the inner conductors connected to the corresponding opposite ridges, similar to the structures in [4–8]. However, a cylindrical circular waveguide rather than a tapered circular or a square waveguide is adopted, thus the complexity of manufacture can be reduced. The end of the quadruple ridges (left side of the OMT in Fig. 1(a)) is terminated with a sunken conical cavity, which decreases the total length as compared with the convex one in [4]. The ridges of the OMT consist of a 45-degree ridge chamfer with a flat surface in the center, different from V-shaped ridges in [11], which helps to suppress some irregular in-band trapped modes. To improve in-band impedance properties, the profile of the tapered ridge has been determined and improved probes with matching rings have been designed. These discussions will be elaborated in Section 3.

3. DESIGN PROCEDURE

This quad-ridged waveguide OMT is based on a cylindrical circular waveguide with an inner-diameter of 192 mm, the same as the dimension of the horn waveguide (with illumination of −13 dB at 56.5°), thus no transition is needed between the OMT and the feed. The preliminary design of the quad-ridged waveguide OMT can be divided into two parts separately:

1. Design of the coaxial to quad-ridged waveguide transition.
2. Design of the smooth transition from the quad-ridged to the circular waveguide transition.

Since no closed-form solution exists for analyzing the quad-ridged shape, the analyses of the coaxial to quad-ridged waveguide transition and the quad-ridged to circular waveguide transition are carried out numerically using the Ansys HFSS code.
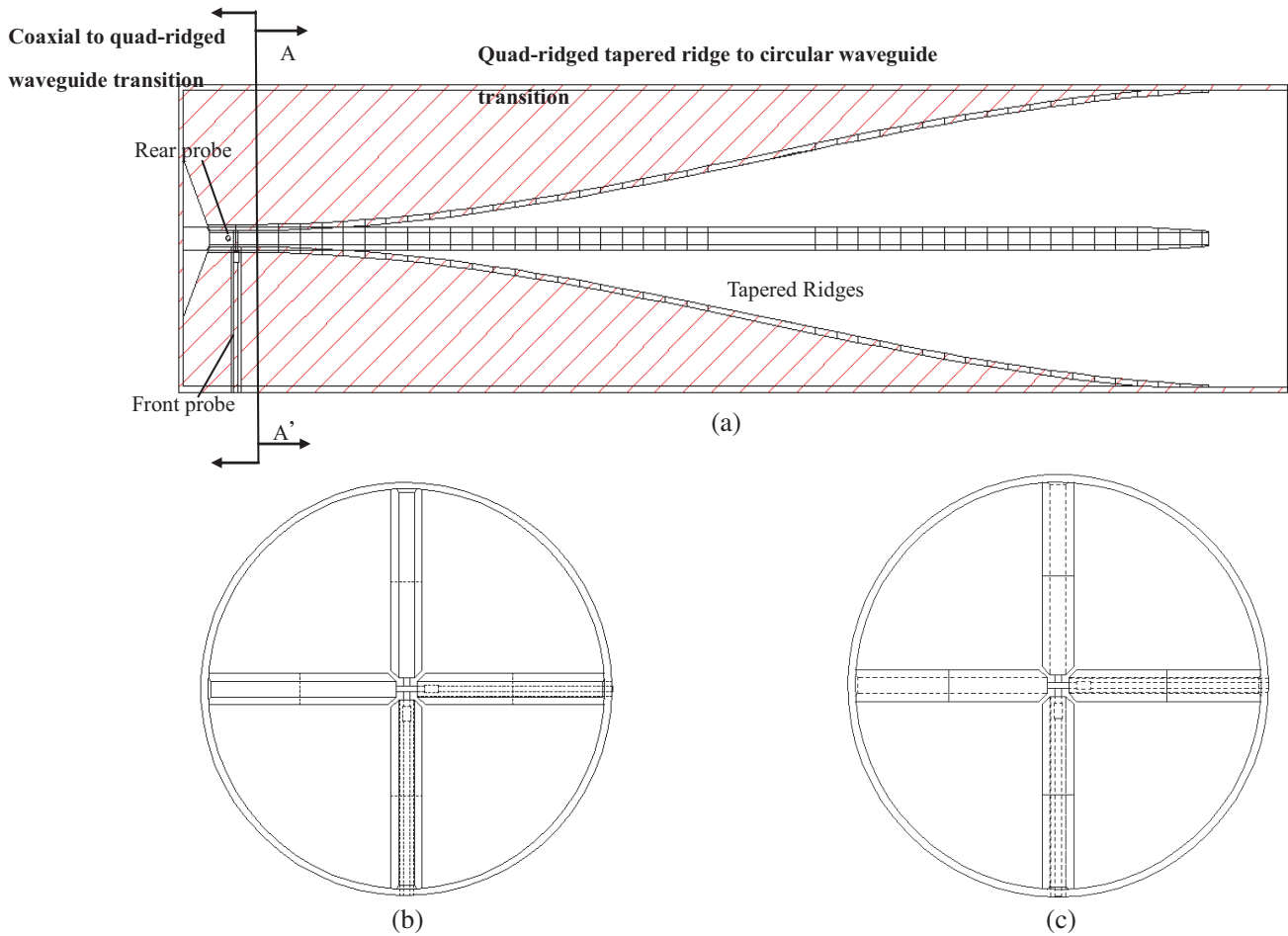
Figure 1. Structure of the L-band quad-ridged waveguide OMT. (a) Cross-sectional view of the OMT (left to AA′ is the coaxial to quad-ridged waveguide transition and right to AA′ is the quad-ridged tapered ridge to circular waveguide transition). (b) Top view. (c) End view with shorting plate removed.

3.1. Design of Coaxial to Quad-Ridged Waveguide Transition

At first, the thickness of the ridges and the gap between opposite ridges in the throat section need to be determined (see Fig. 2(a)). Both the electrical performance, including the mode and impedance properties, and manufacturability are to be ensured. For a single-mode operation, the increase of the bandwidth between the TE_{11} and the $TE_{21}L$ modes and the impedance matching to that of the coaxial cable can be obtained by loading ridges with a very small gap. The quad-ridged waveguide at the coaxial transition (as shown in Fig. 2(a)) consists of a 45-degree ridge chamfer with a flat surface in the center, which enables the gaps between the four ridges to be sufficiently small to have a nearly constant impedance value over the operation frequency range.

At the same time, the way to terminate the back of the waveguide is very critical. The short circuit following the termination of the ridges is shown in Fig. 2(b) to be in the shape of a 45-degree semi-angle cone. It was found to give slightly better performance than a flat back. This can be seen as a matching section from short end to open end. The radius and height of the conical cavity is such that no modes propagate past the ends of the ridges. The end of the ridges is thus very close to an open. In order to match the 50-Ohm coaxial line, initial values of the radius and height of the cone, as well as the location of coaxial probes, can be determined.

The cross section of the quad-ridged waveguide is shown in Fig. 2(a). The ridges have a width of 9.4 mm with a 4.4-mm-flat center and the gap between opposing ridges is 6 mm. As can be seen in Fig. 2(b), the end of four ridges is truncated by a cone with a radius of 57 mm and a height of 18 mm.
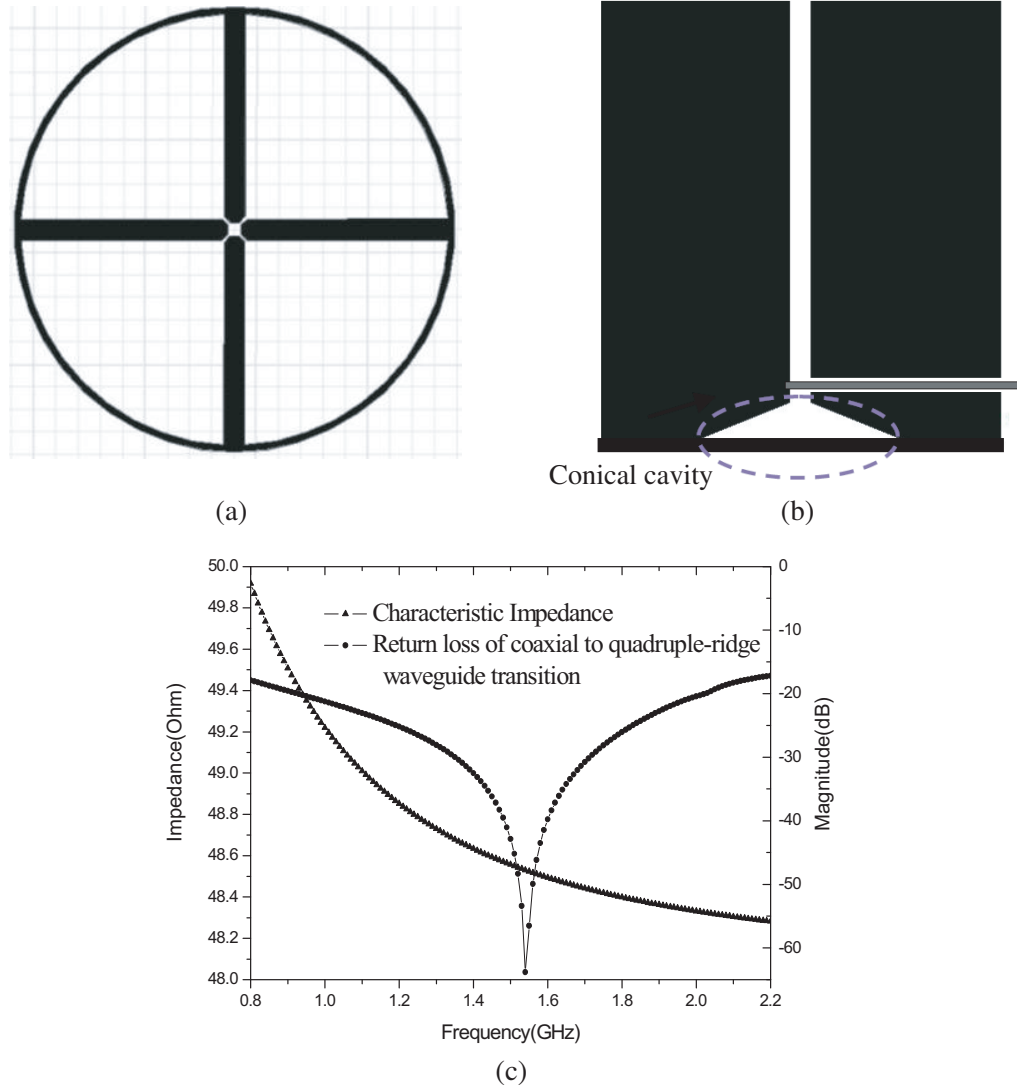
(a)

Conical cavity

(b)

(c)

Figure 2. Coaxial to quad-ridged waveguide transition. (a) Cross section of quad-ridged waveguide. (b) Side view of the ridges ending with the conical cavity. (c) Characteristic impedance and return loss.

Fig. 2(c) shows the characteristic impedance of the quad-ridged section and the return loss of the coaxial to quad-ridged waveguide transition. The impedance of the quad-ridged waveguide is 49.9 ohms and 48.3 ohms for the dominant modes at 0.8 GHz and 2.2 GHz, respectively. From 0.9 GHz to 2 GHz a return loss less than -20 dB can be achieved for this coaxial to quad-ridged waveguide transition.
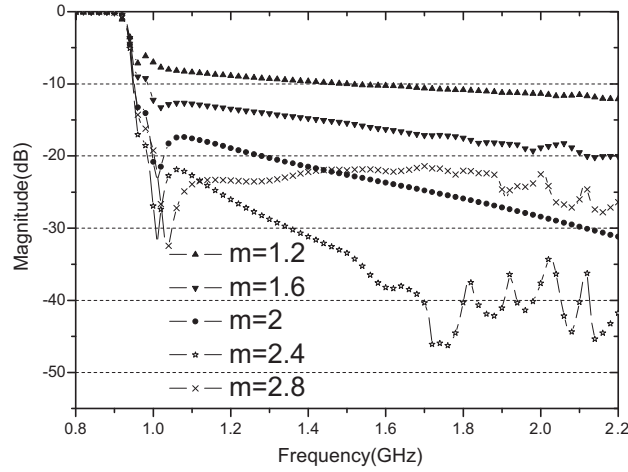
3.2. Design of Quad-Ridged to Circular Waveguide Transition

The profile of the tapered ridges is designed to provide a smooth impedance transition from the chamfered quad-ridged waveguide at the coaxial transition to the circular waveguide near the OMT input. The 192 mm diameter circular waveguide that connects to the antenna feed horn has a cutoff frequency of TE_{11} at 844 MHz. The circular waveguide impedance varies between 656 ohms at 0.95 GHz and 405 ohms at 1.9 GHz, and must be matched simultaneously to the 50-ohm coaxial outputs through the quad-ridged taper transition.

Three types of tapered lines are commonly used for matching transformer transitions: exponential taper, triangular taper and Klopfenstein taper. Klopfenstein impedance taper has been shown to be best in the sense that the reflection coefficient is the lowest over the pass band, and the second best is triangular taper. However, there are steps at the ends of the Klopfenstein tapered section, so the taper
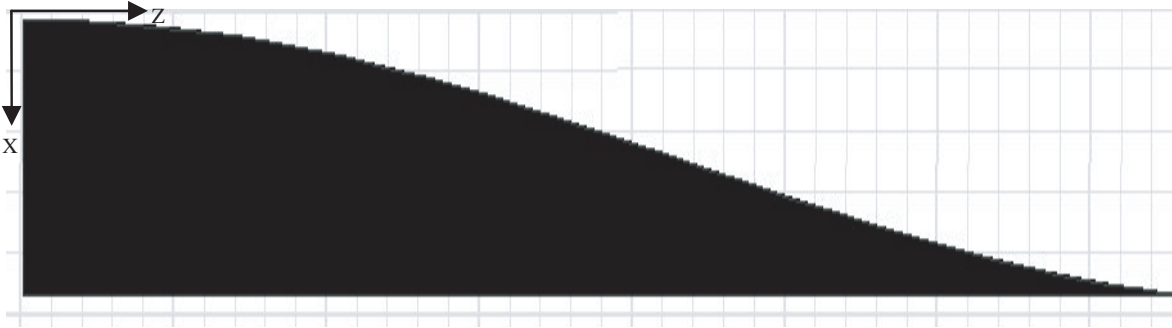
(a)

(b)

Figure 3. Quad-ridged to circular waveguide transition. (a) Ridge taper profile. (b) Return loss for different values of m.

cannot smoothly join the source and load impedances [13]. In this design we choose a triangular taper for the ridges inside the waveguide, as seen in Fig. 3(a), and the function of the taper is as following:

$$x = 93 \times \sin^m(\pi \times z/2/l) \tag{1}$$

A sine-type taper for the ridges in the XZ plane inside the waveguide is given with adjustable parameters m and l, where l is the length of the tapered section. In Equation (1), z is the coordinate in the longitudinal direction and x corresponds to the transverse position of the taper, as seen in Fig. 3(a). A length of 850 mm for l is chosen, and the taper is optimized to give a better and smoother return loss across the operation band by choosing proper values of the parameter m.

The results of the quad-ridged to circular waveguide taper transition with different m values are simulated with the HFSS code. Fig. 3(b) shows the return losses for different values of m from 1.2 to 2.8 in the frequency range of 0.8–2.2 GHz. The position of the first null of the taper response (which occurs at 0.9 GHz as shown in Fig. 3(b)) is determined by the waveguide cutoff and the overall taper length. With the increase of m from 1.2 to 2, the overall return loss gets smaller. As m increases to 2.4, ripples exist in the high frequencies and when m increases to 2.8, the return loss level increases slightly with the ripples still existing in the high frequencies. In this design, the value of m from 2 to 2.4 will be suitable for the taper function and an m value of 2 has been chosen considering the compromise between the lower and smoother return loss across the operation band.

3.3. Full Wave Simulation and Optimization

Combining the two aforementioned components into a single HFSS model yields the overall simulated performance from the circular waveguide input to the coaxial output. Full wave simulation analysis
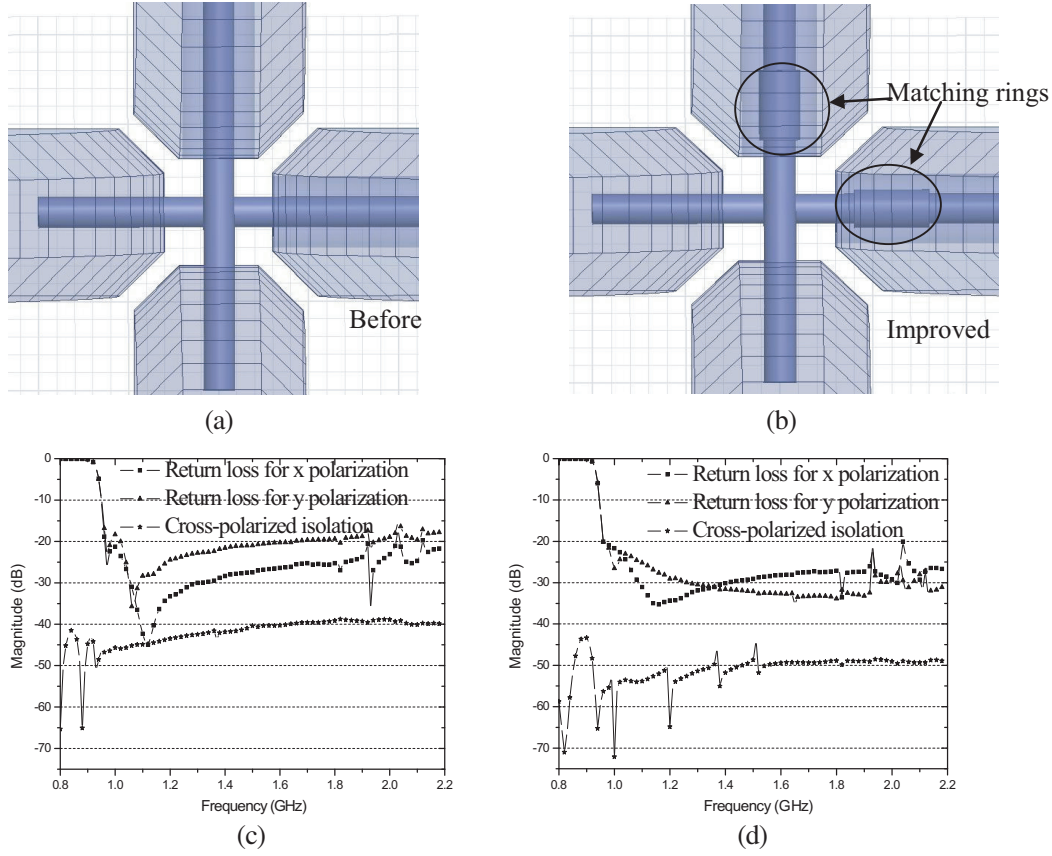
Figure 4. (a) Structure of original OMT with normal probes. (b) Structure of improved OMT with matching rings into the probes. (c) Full wave simulation of two orthogonal polarization ports for original OMT. (d) Full wave simulation of two orthogonal polarization ports for improved OMT.

of two orthogonal polarization ports with normal probes (as shown in Fig. 4(a)) has been carried out. As can be seen in Fig. 4(c), the simulated return loss for x polarization satisfies the -20 dB reflection specification from 0.95 GHz to 1.9 GHz. Because of the different location of the probe for y polarization, the y polarization meets the -20 dB reflection specification only for the frequency range of 1.02 GHz to 1.67 GHz, and the cross-polarized isolation between orthogonal polarizations is lower than 40 dB at the high frequency.

To improve the performance for y polarization and isolation between two orthogonal ports, improved probes have been designed with a matching ring (as seen in Fig. 4(b)). The plot of Fig. 4(d) shows the simulated results for the L-band OMT with improved probes, including the reflection at two orthogonal coaxial ports and the cross-polarized isolation. As can be seen in Fig. 4(d), the simulated OMT performance for y polarization has been improved, with -20 dB reflection levels and the isolation between orthogonal polarizations better than 45 dB from 0.95 GHz to 1.9 GHz. The simulated response meets the return loss and isolation specification by a wide margin.

4. MEASUREMENT OF THE OMT PROTOTYPE

The OMT is constructed from aluminum, with the outer cylindrical waveguide machined and the ridges made by the CNC machine as separate pieces. The L-band prototype OMT is measured connected to a corrugated horn using an Agilent E5071C ENA Series network analyzer as seen in Fig. 5.

The plot of Fig. 6 shows the HFSS simulated and measured results of reflection and cross-polarized isolation properties at two orthogonal coaxial ports for the L-band OMT combined with a corrugated horn. Since the complexity of the OMT is much more sensitive to manufacturing tolerances than the horn, the reflection from the combined system is expected to be dominated by the reflection from the

Figure 5. OMT prototype connected with a corrugated horn for measurement.
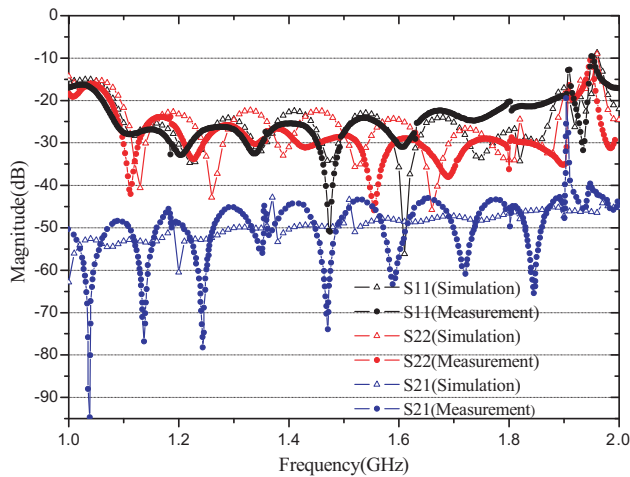

Figure 6. *S* parameter of OMT connected with a corrugated horn (Simulation result with HFSS and measurement result using Agilent E5071C ENA Series network analyzer).
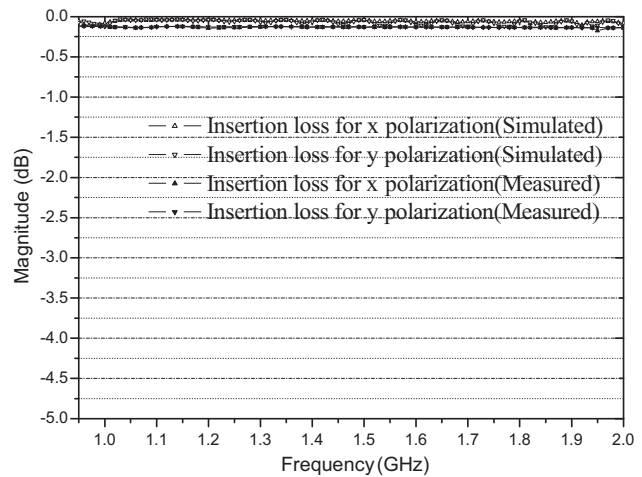

Figure 7. HFSS simulated and measured l-band OMT transmission.

Table 1. Comparison with previous work.

OMT	In Ref. [4]	In Ref. [6]	In Ref. [7]	In Ref. [8]	In Ref. [9]	In Ref. [10]	This work
Bandwidth	2.2 : 1	2 : 1	1.56 : 1	1.7 : 1	2 : 1	3.4 : 1	2 : 1
Return loss (dB)	< -15	< -15	< -25 (Simulation)	< -20	< -18.8	< -15	< -20
Isolation (dB)	> 20	> 25	> 32 (Simulation)	> 40	> 35.7	> 50	> 45
Insertion Loss (dB)	< 0.2	NA	< 0.1 (Simulation)	NA	< 0.2	< 0.2	< 0.15

OMT. The measurement shows a return loss and cross-polarized isolation better than the specifications of -20 dB and 40 dB from 1.1 GHz to 1.9 GHz.

The measured performance is limited by the corrugated horn which works from 1.1 GHz to 1.9 GHz. In fact, the bandwidth of this proposed OMT is from 0.95 GHz to 1.9 GHz, with low-frequency performance limited by the waveguide cutoff and the total length, and high-frequency performance limited by the $TE_{21}L$ trapped-mode resonances.

The plot of Fig. 7 shows the HFSS simulated and measured OMT insertion losses at room

temperature. The measured insertion loss results are averaged from two OMT units connected back-to-back. As expected, the measured insertion loss is higher than the ideal simulated values. The maximum measured insertion loss value is 0.15 dB or better across the entire band. The OMT will be cooled to approximately 70 K, which implies a predicted noise contribution less than 2.2 K.

Compared to the OMT proposed in [4, 6–9] and [10], the OMT in this paper has the advantages of easy design, manufacturability and assembly and also a good comprehensive performance of the bandwidth, return loss, isolation and insertion loss as shown in Table 1.

5. CONCLUSION

The design of a wideband quad-ridged waveguide OMT for the FAST L-band is proposed with a simple design principle by designing two critical OMT parts separately. The design techniques include the size determination of the quad-ridged waveguide, conical cavity and parameter selection of the curve function for the taper transition. In addition, matching rings are introduced into two orthogonal probes to improve the impedance matching and isolation properties. With this design method, the proposed OMT has a bandwidth of 2 : 1 with excellent in-band performance of 20 dB return loss and -45 dB cross-coupling. The insertion loss of this OMT is below 0.15 dB, corresponding to a noise contribution less than 2.2 K while being cooled to 70 K. Compared to the previously proposed OMT, the OMT in this paper has the advantages of easy design, processing and assembly and also has a good comprehensive performance. The design ideas can also be applied to OMT design for other frequency ranges.

ACKNOWLEDGMENT

REFERENCES

1. Bøifot, A. M., E. Lier, and T. Schaug-Pettersen, "Simple and broadband orthomode transducer," *Proc. Inst. Elect. Eng.*, Vol. 137, Pt. H, No. 6, 396–400, Dec. 1990.

2. Reck, T. J. and G. Chattopadhyay, "A 600 GHz asymmetrical orthogonal mode transducer," *IEEE Microw. Wireless Compon. Lett.*, Vol. 23, No. 11, 569–571, Nov. 2013.

3. Robertson, S. D., "Recent advances in finline circuits," *IRE Trans. Microwave Theory Tech.*, Vol. 4, 263–267, 1956.

4. Skinner, S. J. and G. L. James, "Wide-band orthomode transducers," *IEEE Trans. Microwave Theory Tech.*, Vol. 39, 294–300, Feb. 1991.

5. Grimes, P. K., O. G. King, G. Yassin, and M. E. Jones, "Compact broadband planar orthomode transducer," *Electron. Lett.*, Vol. 43, No. 21, 1146–1147, Oct. 2007.

6. Yu, J. L., C. J. Jin, Y. Cao, and H. S. Chen, "Broad-band orthomode transducers," *Proc. Int. Conf. Microwave and Millimeter Wave Technology*, Vol. 1, 320–322, Apr. 2008.

7. Zhuang, Z., B. Li, and Q. Y. Fan, "Design of improved quad-ridged orthomode transducer," *Proc. Int. Conf. Microwave and Millimeter Wave Technology*, 867–870, Jul. 2010.

8. Coutts, G. M., "Octave bandwidth orthomode transducers for the expanded very large array," *IEEE Trans. Antennas Propag.*, Vol. 59, No. 6, 1910–1917, Jun. 2011.

9. De Villiers, D. I. L., P. Meyer, and K. D. Palmer, "Design of a wideband orthomode transducer," *AFRICON 2009*, 1–6, 2009.

10. Dunning, A., M. Bowen, and Y. Chung, "Offset quad ridged ortho-mode transducer with a 3.4 : 1 bandwidth," *2013 Asia-Pacific Microwave Conference Proceedings (APMC)*, 146–148, 2013.

11. Stennes, M., "L-band OMT test report," http://www.nrao.edu/.

12. Nan, R., "Five hundred meter aperture spherical radio telescope (FAST)," *Sci. China Ser. G*, Vol. 49, No. 2, 129–148, 2006.

13. Pozar, D. M., *Microwave Engineering*, 3rd edition, John Wiley & Sons Inc., 2005.